

## Quarter-Wave Plates and X-ray Magnetic Circular Dichroism on ID24 at the ESRF

S. Pizzini,<sup>a\*</sup> M. Bonfim,<sup>a</sup> F. Baudalet,<sup>b</sup> H. Tolentino,<sup>a</sup> A. San Miguel,<sup>c</sup> K. Mackay,<sup>a</sup> C. Malgrange,<sup>d</sup> M. Hagelstein<sup>c</sup> and A. Fontaine<sup>a</sup>

<sup>a</sup>Laboratoire Louis Néel, CNRS, BP 166, 38042 Grenoble CEDEX, France, <sup>b</sup>LURE, Bâtiment 209D, Centre Universitaire, 91405 Orsay CEDEX, France, <sup>c</sup>ESRF, BP 220, 38043 Grenoble CEDEX, France, and <sup>d</sup>Laboratoire de Minéralogie-Cristallographie, Université Paris 6 et 7, 75252 Paris CEDEX 05, France. E-mail: pizzini@labs.polycnrs-gre.fr

(Received 7 January 1998; accepted 16 March 1998)

The first XMCD measurements carried out on the ID24 energy-dispersive XAS beamline at the ESRF are reported. Circular-polarized X-rays are obtained using perfect diamond crystals as quarter-wave plates. The very small source divergence allows circular polarizations close to unity to be obtained.

**Keywords:** X-ray magnetic circular dichroism; X-ray quarter-wave plates.

### 1. Introduction

X-rays with a high rate of circular polarization ( $P_c$ ) are essential for X-ray magnetic circular dichroism, which measures the difference of absorption of right- and left-handed X-rays of an element-selected ferromagnetic sublattice and relates it to the magnetic moment of the selected atom (Goulon *et al.*, 1997). In first- and second-generation synchrotron radiation sources using bending-magnet devices, circular polarization (left or right) is obtained by selecting the radiation emitted above or below the synchrotron orbit plane. This configuration implies a considerable flux loss and a large uncertainty on the polarization rate. At third-generation sources like the ESRF, X-rays of tunable polarization can be obtained using specific insertion devices like helical undulators (Yamamoto & Kitamura, 1987; Elleaume, 1990; Sasaki, 1993).

An alternative way to tune the X-ray polarization is to use perfect crystals as phase plates. The birefringence of a perfect crystal at or close to Bragg diffraction conditions is predicted by dynamical theory. The difference  $n_\sigma - n_\pi$  between the refractive index of the  $\sigma$  and  $\pi$  components of the incoming electric field depends on the angular departure from the Bragg angle,  $\Delta\theta$ . In their first conception, phase plates took advantage of the birefringence of X-rays inside the reflection profile. Since the birefringence varies rapidly with  $\Delta\theta$ , highly collimated X-ray beams are required (Golovchenko *et al.*, 1986).

Phase plates can also be used outside the reflection profile using the 'non-deviated' forward-diffracted beam. Such a set-up was first used with a thin silicon crystal and a well collimated beam (Hirano *et al.*, 1991, 1992). The birefringence is smaller than that inside the reflection profile but its variation with  $\Delta\theta$  is slower (Dmitrienko & Belyakov, 1980). This offers the possibility to work with

divergent X-ray beams. Thanks to their low absorption coefficient, rather thick diamond phase plates can be used with this set-up. This explains the rapid development of diamond quarter-wave plates (QWP) working far from crystal reflection in Bragg (Giles *et al.*, 1993; Giles, Malgrange, Goulon, de Bergevin, Vettier, Dartyge, Fontaine, Giorgetti & Pizzini, 1994) and Laue (Giles, Malgrange, Goulon, de Bergevin, Vettier, Dartyge, Fontaine & Pizzini, 1994) geometry.

The principles of QWP have been detailed by Giles, Malgrange, Goulon, de Bergevin, Vettier, Dartyge, Fontaine, Giorgetti & Pizzini (1994) and Giles, Malgrange, Goulon, de Bergevin, Vettier, Dartyge, Fontaine & Pizzini (1994). Only the basic concepts are summarized here. It is known that if the diffraction plane of the birefringent crystal is set at an angle  $\Psi$  with respect to the electric field of the linearly polarized X-ray beam incident on the crystal, the circular polarization rate  $P_c$  of the transmitted wave depends on the phase shift  $\Phi$  between the two components  $E_\sigma$  and  $E_\pi$ ,

$$P_c = (I_R - I_L)/(I_R + I_L) = \sin 2\Psi \sin \Phi. \quad (1)$$

The transmitted beam is fully circularly polarized when  $\Psi = 45^\circ$  and  $\Phi = 90^\circ$ . This is the QWP configuration. Far from Bragg conditions, the phase shift  $\Phi$  between the  $\sigma$  and  $\pi$  components of the electric field depends on the crystal thickness and on the offset  $\Delta\theta$ , *i.e.* on the angular difference between the incident angle and the centre of the diffraction profile,

$$\Phi = (2\pi/\lambda)(n_\sigma - n_\pi) = r_e^2 \text{Re}[F_h F_h^-] \lambda^3 \sin(2\theta_B) t / 2\pi V^2 \Delta\theta, \quad (2)$$

where  $t$  is the beam path in the crystal,  $r_e$  is the classical electron radius,  $V$  is the volume of the unit cell and  $F_h$  is the structure factor of the  $hkl$  reflection.

Quarter-wave-plate conditions can therefore be obtained by turning the crystal away from the reflection profile by an angle

$$\Delta\theta_{\pi/2} = r_e^2 \text{Re}[F_h F_h^-] \lambda^3 \sin(2\theta_B) t / \pi^2 V^2. \quad (3)$$

The angular dependence of the circular polarization rate can then be simply expressed as a function of  $\Delta\theta_{\pi/2}$  as

$$P_c = \sin 2\Psi \sin[(\pi/2)(\Delta\theta_{\pi/2}/\Delta\theta)]. \quad (4)$$

For an X-ray beam with angular divergence  $\alpha$ , the circular polarization rate deduced from (1) and (2) for a certain angular offset  $\Delta\theta$  has to be convoluted with a Gaussian function of width  $\alpha$ . In order to minimize the effect of the X-ray beam divergence on  $P_c$ ,  $\Delta\theta_{\pi/2}$  should be maximized so that it falls into a region where the phase shift  $\Phi$  changes more slowly with  $\Delta\theta$ . This can be obtained by increasing the crystal thickness, at the expense of transmission. It follows that light non-absorbing crystals should be used.

In the present work a 0.74 mm-thick diamond crystal was used as a phase plate on the energy-dispersive X-ray absorption beamline at the ESRF (ID24) (Hagelstein *et al.*, 1997). The aim of this development is to allow XMCD to be carried out on a beamline where the planar undulator produces a strictly linearly polarized beam. The undulator fundamental can be tuned between 4.5 keV and 8 keV, while the spectral range from 8 to 25 keV is accessible using the second or higher undulator harmonics. A curved Si(111) crystal in Bragg configuration was used as a dispersive polychromator. A polychromatic focus of  $30 \times 100 \mu\text{m}$  is obtained using a four-point bender. The particular contour of the crystal minimizes optical aberrations (Pellicer-Porres *et al.*, 1998). The energy-dispersive spectrometer is arranged in a  $\theta-2\theta$  set-up. The detector is a CCD camera made of  $512 \times 512$  pixels and lens coupled to a scintillation screen which receives the X-ray photons (Koch *et al.*, 1995).

Previous tests aiming to assess the possibility of installing a QWP on an energy-dispersive spectrometer have been carried out at LURE. Due to the large divergence of the DCI source ( $\sim 80$  arcsec), the circular polarization rate of the beam transmitted by the plate was of the order of 60% at 7 keV (Giles *et al.*, 1993; Giles, Malgrange, Goulon, de Bergevin, Vettier, Dartyge, Fontaine, Giorgetti & Pizzini, 1994; Giles, Malgrange, Goulon, de Bergevin, Vettier, Dartyge, Fontaine & Pizzini, 1994). This was sufficient to measure high-quality  $L_{2,3}$ -edge XMCD spectra of heavy rare earths. On the other hand, we showed that at the Ho  $L_3$ -edge the X-ray intensity transmitted by the diamond was a factor of three larger than that available when moving outside the orbit plane by the amount necessary to obtain the same  $P_c$ .

In this experiment, as in most experiments performed at LURE, the (111) diamond crystal was operated in the asymmetric Laue geometry using the  $(11\bar{1})$  diffracting planes which make a  $19.47^\circ$  angle with the  $[111]$  direction normal to the phase plate. For energies around the  $L_{2,3}$ -

edges of rare earths from Gd to Ho, the Bragg angles fall at around  $20^\circ$  and the X-ray beam has an almost normal incidence on the diamond entrance face. The transmission of the plate is  $\sim 0.2$  at the Gd  $L_3$  edge.

The diamond crystal is installed close to the polychromatic focus point of the Si crystal. The main constraint of the energy-dispersive set-up is that the different energies diffracted by the curved Si crystal should satisfy Bragg's law simultaneously on the diamond crystal. This is equivalent to a condition of non-dispersivity between the two crystals which can be written as

$$\tan \theta_2 / \tan \theta_1 = 2(1 - qb/p)^{-1} \cos \Psi, \quad (5)$$

where  $\theta_1$  and  $\theta_2$  are the Bragg angles on the polychromator and the phase plate, respectively, for the mean energy.  $b$  is related to the angle of asymmetry,  $\alpha$ , of the reflecting planes on the polychromator by the relation  $b = \sin(\theta - \alpha) / \sin(\theta + \alpha)$ .  $p$  is the distance between the source and the crystal,  $q$  is the distance between the crystal and the focus point. This equation links the lattice parameters of the reflection planes used on the first and the second crystal and contains as parameter the angle  $\Psi$  between the two diffraction planes.

In order to achieve optimized conditions,  $\Psi$  can be varied with respect to the ideal  $45^\circ$  value at the expense of  $P_c$  (equation 4). It can be shown that, for the chosen configuration and for energies between 7 and 9 keV, the  $\Psi$

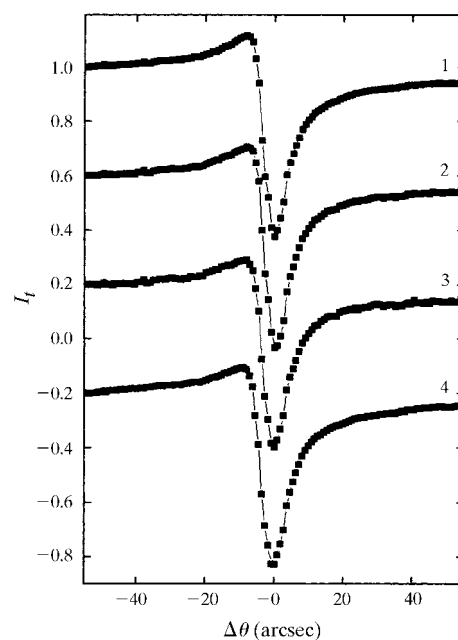


**Figure 1**

Angular dependence of the X-ray intensity transmitted by the diamond crystal close to Bragg conditions, measured for the four energy windows close to the Gd  $L_3$  edge, specified in Fig. 2. The angle  $\Psi$  was adjusted to obtain optimum non-dispersivity conditions: Bragg conditions are met at the same time in the four energy regions. The transmitted intensity is normalized to unity before the Bragg angle and it is artificially shifted vertically for three of the four energy regions.

values fall between  $40$  and  $50^\circ$  giving a circular polarization rate larger than  $0.985$ .

In Fig. 1 we show, close to Bragg conditions and for four energy windows around the Gd  $L_3$  edge ( $7243$  eV), the angular dependence of the X-ray intensity transmitted by the diamond crystal. The anomalous increase of the transmission before the Bragg reflection is due to the Borrmann effect (Batterman, 1964). The occurrence of this effect is an indication of the high quality of the diamond crystal. The minimum in the transmitted photons corresponds to the loss of intensity associated with diffraction conditions. In order to optimize the non-dispersivity conditions, the transmitted intensity was measured in four energy regions across the absorption edge (specified in Fig. 2). The angle  $\Psi$  was optimized in order to obtain the same Bragg angle for the four energy windows. This could be performed with a sensitivity of  $0.1^\circ$  and  $\Psi$  was found to be approximately  $41^\circ$ .

The ferromagnetic samples for XMCD experiments were set at the spectrometer focus point, between the poles of a  $1.05$  T NdFeB permanent magnet built by Magnetic Solutions. The magnetic field direction can be rapidly ( $<1$  s) switched from parallel to antiparallel to the X-ray propagation direction, thanks to a rotation stage operated by compressed air.

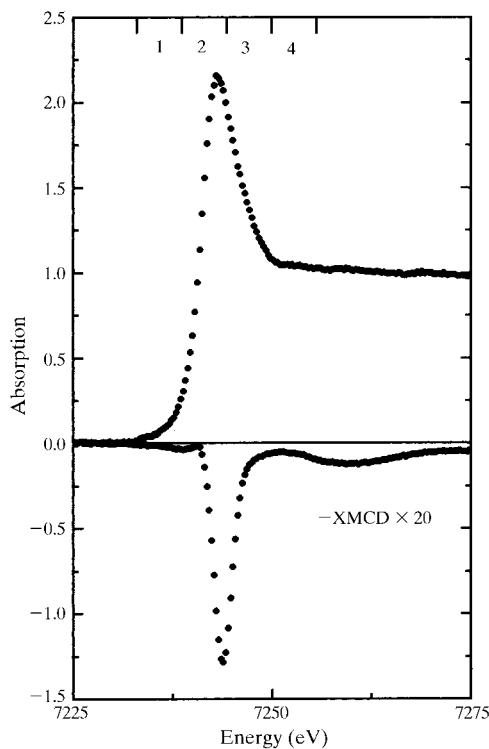


**Figure 2**

Gd  $L_3$ -edge total X-ray absorption and XMCD spectrum of a GdCo<sub>5</sub> amorphous film measured at  $300$  K. The XMCD signal is multiplied by  $-20$ . A signal-to-noise ratio better than  $400$  was obtained after  $100$  min acquisition time. A signal-to-noise ratio larger than  $100$  can be obtained in a few minutes. Non-dispersivity conditions were optimized for the energy windows 1 to 4 (see Fig. 1).

The Gd  $L_3$ -edge XMCD spectrum measured with the diamond plate for a GdCo<sub>5</sub> amorphous film is shown in Fig. 2. The amplitude of the XMCD signal is almost twice as large as that obtained at LURE on the same sample (Rueff, 1996). Thanks to the extremely small divergence of the beam emitted by the ESRF undulator, the circular polarization rate delivered by the QWP is largely improved with respect to our previous experiments at LURE.

In order to better characterize the efficiency of the diamond phase plate, XMCD measurements were carried out for several incident angles corresponding to offsets between  $-110$  and  $+110$  arcsec. The variation of the XMCD amplitude with  $\Delta\theta$  is a measure of the circular polarization rate. The absolute circular polarization rate of the X-rays transmitted by the QWP could be obtained by comparison with theoretical values, convoluted with a Gaussian function which takes into account the X-ray divergence. The comparison of measurement and theory is shown in Fig. 3 for the Gd  $L_3$  signal of the GdCo<sub>5</sub> film. The best agreement is obtained supposing a source divergence of the order of  $4.5$  arcsec which is consistent with the characteristics of the beamline. Note that the maximum polarization rate obtained under quarter-wave-plate conditions, at  $\pm 75$  arcsec, is of the order of  $0.99$ , in agreement with the value expected from (1) for  $\Psi \simeq 41^\circ$ . Note that, consistent with the very small beam divergence, a very high degree of circular polarization is also obtained for offsets of  $\pm 25$  arcsec corresponding to three-quarter-wave-plate conditions.

In a classical set-up, *i.e.* on a bending-magnet beamline, it is not so straightforward to change the X-ray helicity. The XMCD measurement is therefore carried out with a fixed helicity and by measuring the difference of absorption for opposite directions of the applied magnetic field [ $\mu(+B) - \mu(-B)$ ]. When using this set-up, the applied magnetic field

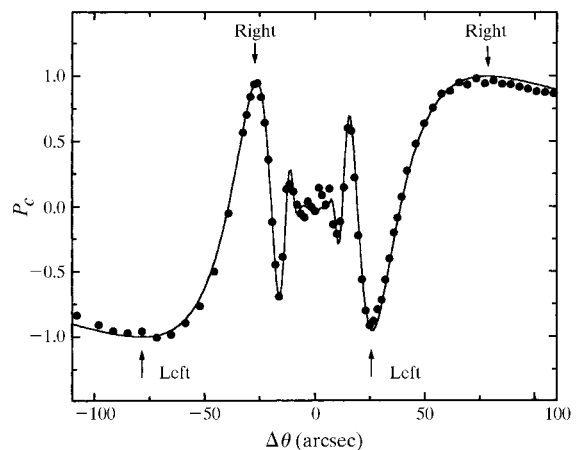


**Figure 3**

The angular dependence of the measured Gd  $L_3$ -edge XMCD amplitude (circles) is fitted to the angular dependence of the circular polarization rate (equation 4) (full line) convoluted with a Gaussian function of width  $4.5$  arcsec. Angular offsets of  $\pm 75$  and  $\pm 25$  arcsec correspond to quarter-wave-plate and three-quarter-wave-plate conditions, respectively.

has to exceed the coercive field of the studied sample in order to reverse the magnetization. When using a quarter-wave plate, the X-ray helicity can be switched from right to left by flipping the offset from positive to negative; we measure  $[\mu^R - \mu^L]$ . The advantage of this set-up is that the applied field can be used as a degree of freedom; element-selective magnetization and hysteresis curves can then be measured (Chen *et al.*, 1993; Pizzini *et al.*, 1997). We have already shown that the signal measured this way is the superposition of XMCD and a residual non-magnetic term, deriving mainly from the different absorption of the QWP in the two angular positions (Giles, 1995). This term can be eliminated by carrying out two ‘flipping’ measurements  $\{[\mu^R(+B) - \mu^L(+B)]$  and  $[\mu^R(-B) - \mu^L(-B)]\}$  with fixed fields of opposite directions. The half-difference of these

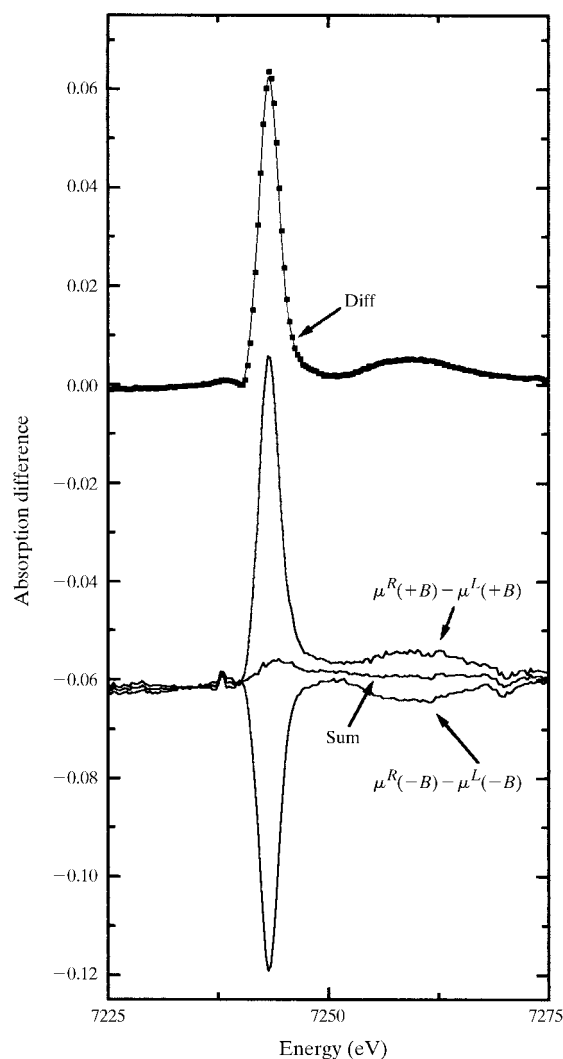


**Figure 4**

The difference spectrum  $[\mu^R - \mu^L]$  ( $R$  = right,  $L$  = left) obtained by flipping the QWP offset between  $\pm 75$  arcsec is measured with applied fields  $+B$  and  $-B$  at the Gd  $L_3$  edge. The half-difference of the two spectra (Diff, full line) is identical to the XMCD signal obtained as  $[\mu^R(+B) - \mu^R(-B)]$  (squares). The residual signal (Sum) derives mainly from the different absorption of the diamond crystal at  $\pm \Delta\theta$ .

two measurements recovers the XMCD signal, as the non-magnetic background is the same in the two cases.

In Fig. 4 we show the  $[\mu^R - \mu^L]$  spectra obtained for GdCo<sub>5</sub> by alternating the diamond crystal between two quarter-wave-plate offsets of  $\pm 75$  arcsec, corresponding to maximum and equal right and left helicities (see Fig. 3). The spectra were measured twice, with fixed field  $+B$  and  $-B$  applied parallel and antiparallel, respectively, to the X-ray propagation direction. The half-difference of these two spectra is indeed identical to the XMCD signal measured by reversing the applied field direction (Fig. 4). The half-sum is the field-independent background mentioned above. The non-magnetic origin of this signal is confirmed by the fact that the same effect is observed when  $[\mu^R - \mu^L]$  is measured for the same sample in an unmagnetized state. Fig. 1 shows that, close to Bragg conditions, the X-ray intensity transmitted by the diamond crystal is different for two opposite offset values. This effect gives the observed shift of the XMCD baseline as  $-6 \times 10^{-2}$  (Fig. 4). Close to the edge the structures in the background signal are sample specific. X-rays emerging from the crystal at a slightly different angle and position cause a slight shift of the energy scales in the two geometries. This gives a derivative-like signal at the edge, to which the effect of sample

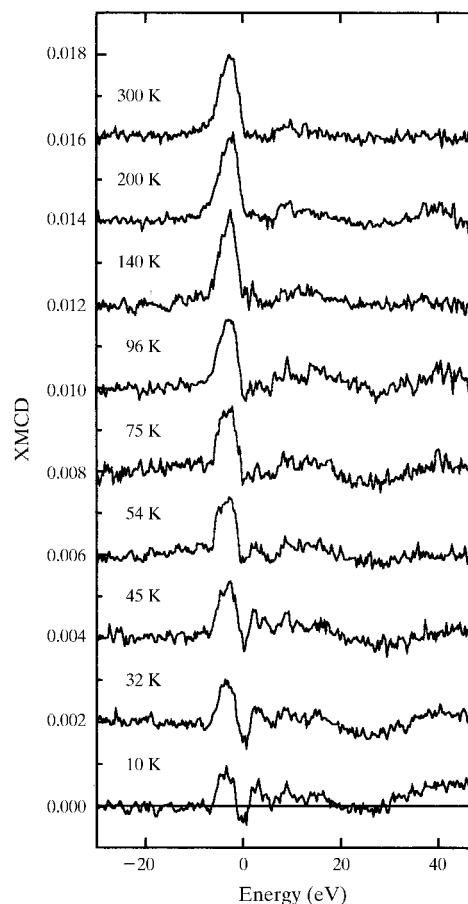


**Figure 5**

Temperature-dependent Ce  $L_3$ -edge XMCD signal measured for a CeH<sub>16</sub>Å/Fe<sub>16</sub>Å multilayer.

defects will have to be added. Fig. 4 shows that the effect is of the order of some  $10^{-3}$  at the edge. This is small compared with the magnitude of the  $L_{2,3}$  XMCD signal for rare earths but becomes important when  $K$  edges of  $3d$  transition metals are measured.

## 2. Applications

As examples of application of this set-up we describe two experiments recently carried out on the ID24 beamline.

### 2.1. Polarization of Ce 5d states in CeH/Fe multilayers

Ce  $L_{2,3}$ -edge (6.1 and 5.7 keV) XMCD spectra were measured for a series of hydrided CeH/Fe multilayers. Fig. 5 shows the temperature-dependent Ce  $L_{3}$ -edge XMCD signal carried out for a  $\text{CeH}_{16\text{Å}}/\text{Fe}_{16\text{Å}}$  sample. These hydrided heterostructures present magnetic properties very different from those previously studied for non-hydrided multilayers (Klose *et al.*, 1994). They present a strong perpendicular anisotropy at low temperatures and magnetic coupling of Fe across the CeH layers (Bauer *et al.*, 1994; Schulte *et al.*, 1995). The spectra were recorded between 10 K and 300 K using a closed-cycle refrigerator.

For this experiment a 200  $\mu\text{m}$ -thick diamond (100) crystal was used. With the angle between the (111) planes and the crystal normal being  $35.26^\circ$ , an almost normal incident geometry is obtained at the Ce  $L_{2,3}$  edges, where the Bragg angles are  $\sim 32$  and  $29^\circ$ . The transmission of the crystal at 6 keV is  $\sim 0.5$ . The offsets for quarter-wave-plate conditions are  $\pm 50$  arcsec.

Each spectrum was obtained in the ‘classical’ way by switching the direction of the magnetic field, keeping a fixed helicity. The spectra in Fig. 5 are the result of 51 field inversions, for a total acquisition time of 20 min. A good signal-to-noise ratio is obtained even for the low-temperature signal, where the magnitude of the XMCD signal is only  $1.5 \times 10^{-3}$ .

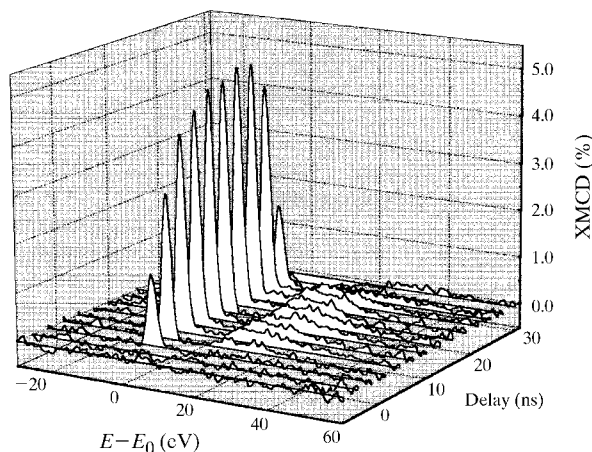


**Figure 6**  
Time-evolution of the Gd  $L_{3}$ -edge XMCD signal of a  $\text{GdCo}_3$  film during and after a 22 ns field pulse. The zero of the delay time corresponds to the start of the magnetic field pulse.

The presence of an XMCD signal at the Ce  $L_{3}$  edge at 300 K indicates that the Ce 5d states are magnetically polarized. The presence of a single-peak structure is in contrast with the double-peak structure found for the XMCD signal in non-hydrided samples (Klose *et al.*, 1994). This would indicate a relocation of 4f states in this system. Details of this experiment will be reported in a future paper (Arend *et al.*, 1998).

### 2.2. Nanosecond-resolved XMCD measurements

Taking advantage of the time structure of the X-ray beam in single-bunch operation mode, we were able to carry out the first nanosecond-resolved XMCD measurements (Bonfim *et al.*, 1998). Circular polarization at the Gd  $L_{3}$  edge was obtained using the 0.74 mm-thick diamond (111) quarter-wave plate.

The experiment is conceived as a pump-probe scheme. The pump is a pulsed magnetic field of a few nanoseconds, generated by microcoils at the 357 kHz ESRF frequency. The hairpin-shaped 50  $\mu\text{m}$ -thick copper microcoil with a 50  $\mu\text{m}$ -wide gap takes full advantage of the focusing optics (a spot size as small as  $30 \times 100 \mu\text{m}$ ) of the energy-dispersive XAS spectrometer. 25 ns-long pulses of 100 A current generate 0.4 T-high magnetic field pulses.

The probe is a 100 ps-long X-ray pulse processed by an energy-dispersive X-ray absorption spectrometer. The single-bunch filling allows the delay between the pump and the probe to be tuned from 0 to 2.8  $\mu\text{s}$ , the temporal distance between two X-ray bunches. A series of XMCD measurements were carried out, each corresponding to a particular delay between the X-ray bunch and the magnetic pulse. The XMCD signal was obtained as the difference of two absorption spectra collected with right and left circular polarizations. The two helicities were obtained by flipping the quarter-wave plate from one side of the (111) Bragg profile to the other. The XMCD signal is a result of photons from a few hundred million bunches, each of which has the same phase relationship with the magnetic pulse.

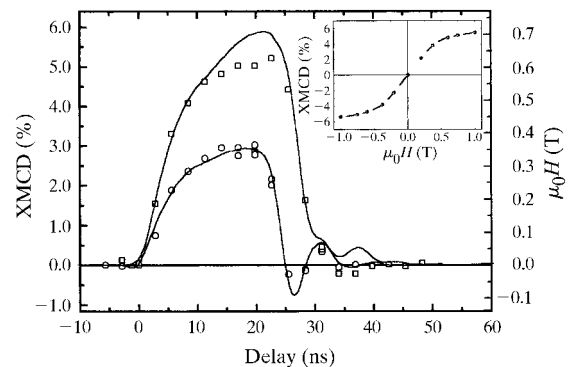


**Figure 7**  
The time-evolution of the Gd  $L_{3}$ -edge XMCD amplitude of  $\text{GdCo}_3$  (circles and squares) is compared with the field pulse (full lines) for two intensities of the field pulse (0.3 and 0.7 T). In the inset the amplitude of the XMCD signal obtained with a static field from  $-1$  T to 1 T is shown.

In this first investigation we have analyzed the time response of a GdCo<sub>3</sub> amorphous thin film grown by sputtering at the Laboratoire Louis Néel. The film is slightly anisotropic with the easy axis of magnetization in the plane of the film. The pulsed field produced by the microcoil is applied perpendicular to the film, along the X-ray propagation direction. In this scheme the 100 ps-long X-ray bunch probes progressive magnetization during and after the magnetic pulse. Details of this experiment are described by Bonfim *et al.* (1998).

In Fig. 6 we show the time evolution of the XMCD signal during and after a 22 ns-long 0.7 T field pulse. The acquisition time for each spectrum is approximately 3 min, during which the QWP offset was reversed 11 times. In Fig. 7 the amplitude of the XMCD intensity for two amplitudes of the field pulses (0.3 and 0.7 T) is reported together with the time evolution of the field pulse. The magnetization of the GdCo<sub>3</sub> film closely follows the current, which indicates that the characteristic time for spin rotation from the parallel to perpendicular direction is smaller than 10<sup>-9</sup> s.

We thank Professor W. Felsch of Göttingen University for letting us present the data on CeH/Fe multilayers, C. M. Giles of LNLS Campinas for help in setting up the QWP, Thomas Neisius of ESRF for help on the beamline, and Sebastian Pasternak of ESRF for technical support. We are also grateful to Professor A. R. Lang (Bristol University) and Professor T. Ishikawa (Spring-8) for kindly lending us the diamond crystals. The experimental work at the ESRF has been performed with the approval of the Program Advisory Committee (proposal HE-004).

## References

- Arend, M., Felsch, W., Krill, G., Delobbe, A., Baudelet, F., Dartyge, E., Kappler, J.-P., Finazzi, M., Pizzini, S., Fontaine, A. & San Miguel-Fuster, A. (1998). Submitted.
- Batterman, B. W. (1964). *Rev. Mod. Phys.* **36**, 681–716.
- Bauer, Ph., Klose, F., Schulte, O. & Felsch, W. (1994). *J. Mag. Mag. Mater.* **138**, 163–172.
- Bonfim, M., Mackay, K., Pizzini, S., San-Miguel, A., Tolentino, H., Giles, C., Neisius, T., Hagelstein, A., Baudelet, F., Malgrange, C. & Fontaine, A. (1998). *J. Synchrotron Rad.* **5**, 750–752.
- Chen, C. T., Idzerda, Y. U., Lin, H.-J., Meigs, G., Chaiken, A., Prinz, G. A. & Ho, G. A. (1993). *Phys. Rev. B*, **48**, 642–645.
- Dmitrienko, V. E. & Belyakov, V. A. (1980). *Sov. Technol. Phys. Lett.* **6**, 621–622.
- Elleau, P. (1990). *Nucl. Instrum. Methods*, **A291**, 371–377.
- Giles, C. (1995). PhD thesis, Université Paris 7 – Denis Diderot, France.
- Giles, C., Malgrange, C., Goulon, J., de Bergevin, F., Vettier, C., Dartyge, E., Fontaine, A., Giorgetti, C. & Pizzini, S. (1993). *Acta Cryst.* **A49**, C377.
- Giles, C., Malgrange, C., Goulon, J., de Bergevin, F., Vettier, C., Dartyge, E., Fontaine, A., Giorgetti, C. & Pizzini, S. (1994). *J. Appl. Cryst.* **27**, 232–240.
- Giles, C., Malgrange, C., Goulon, J., de Bergevin, F., Vettier, C., Dartyge, E., Fontaine, A. & Pizzini, S. (1994). *Nucl. Instrum. Methods*, **A349**, 622–625.
- Golovchenko, J. A., Kincaid, B. M., Levesque, R. A., Meixner, A. E. & Kaplan, D. R. (1986). *Phys. Rev. Lett.* **57**, 202–205.
- Goulon, J., Goulon-Ginet, C. & Brookes, N. B. (1997). Editors. *Proceedings of the 9th International Conference on XAFS*, Grenoble, August 1996.
- Hagelstein, M., San-Miguel, A., Fontaine, A. & Goulon, J. (1997). *J. Phys. IV*, **7(C2)**, 303–308.
- Hirano, K., Izumi, K., Ishikawa, T. & Kikuta, S. (1991). *Jpn. J. Appl. Phys.* **30**, L407.
- Hirano, K., Kanzaki, K., Mikami, M., Tamasaku, K., Ishikawa, T. & Kikuta, S. (1992). *J. Appl. Cryst.* **25**, 531.
- Klose, F., Schulte, O., Rose, F., Felsch, W., Pizzini, S., Giorgetti, C., Baudelet, F., Dartyge, E., Krill, G. & Fontaine, A. (1994). *Phys. Rev. B*, **50**, 6174–6183.
- Koch, A., Hagelstein, M., San-Miguel, A., Fontaine, A. & Ressler, T. (1995). *Proc. SPIE*, **2416**, 85–93.
- Pellicer-Porres, J., San-Miguel, A. & Fontaine, A. (1998). *J. Synchrotron Rad.* **5**, 1250–1257.
- Pizzini, S., Fontaine, A., Garcia, L. M., Bobo, J.-F., Picuch, M., Baudelet, F., Malgrange, C., Alimoussa, C., Snoeck, E. & Casanove, M. J. (1997). *J. Mag. Mag. Mater.* **166**, 38–44.
- Rueff, J. P. (1996). PhD thesis, Université J. Fourier, Grenoble, France.
- Sasaki, S. (1993). *Nucl. Instrum. Methods*, **A331**, 763–767.
- Schulte, O., Klose, F. & Felsch, W. (1995). *Phys. Rev. B*, **52**, 6480–6488.
- Yamamoto, S. & Kitamura, H. (1987). *Jpn. J. Appl. Phys.* **26**(10), L1613–L1615.